scientific data

Check for updates

OPEN

DATA DESCRIPTOR

A Forcecardiography dataset with simultaneous SCG, Heart Sounds, ECG, and Respiratory signals

Salvatore Parlato[1], Jessica Centracchio[1]✉, Eliana Cinotti[1], Maria Virginia Manzi[2], Grazia Canciello[2], Maria Prastaro[2], Maria Lembo[2], Benjamin M. Brandwood[3], Gaetano D. Gargiulo[3], Paolo Bifulco[1], Giovanni Esposito[2], Raffaele Izzo[2] & Emilio Andreozzi[1]

FOSTER is the first ever publicly available dataset of forcecardiography (FCG) signals with simultaneous recordings of conventional seismocardiography (SCG), phonocardiography (PCG), electrocardiography (ECG), and respiratory signals. The dataset contains recordings from 40 participants (20 males and 20 females) and aims to foster and facilitate research on non-invasive cardio-respiratory monitoring using mechanical sensors. All signals were acquired simultaneously to ensure precise temporal alignment for accurate analysis. Each recording lasts about 7 minutes and includes both long phases of quiet breathing and short phases of inspiratory and expiratory apneas. The open accessibility of the FOSTER dataset aims to facilitate advancements in unobtrusive cardio-respiratory patient monitoring, support the development of novel diagnostic tools and algorithms to detect specific events of the cardiac and respiratory cycles, and help researchers to explore the potential of combined electrical and mechanical cardiac monitoring.

Background & Summary

Non-invasive cardiomechanical monitoring techniques, such as Seismocardiography (SCG)[1–4], Gyrocardiography (GCG)[5,6], Phonocardiography (PCG)[7–9], Ballistocardiography (BCG)[10–16], provide valuable insights into the mechanics of the heart, offering a promising approach to ubiquitous cardiovascular assessment. These techniques record the mechanical vibrations and acoustic emissions generated by the heart contraction via small, lightweight mechanical sensors. SCG records the chest wall vibrations caused by the cardiac activity via MEMS accelerometers, which enables continuous cardiomechanical monitoring, also in wearable applications[17,18]. GCG measures cardiac-induced rotational movements of the chest surface via MEMS gyroscopes, which measure angular velocity and provide complementary data to SCG[5,6]. Accelerometers and gyroscopes combined in a single Inertial Measurement Unit (IMU) may offer a more detailed and accurate representation of heart mechanics and respiration providing an integrated SCG and GCG monitoring[19–23].

Several datasets of SCG, GCG, and PCG signals are available, which generally include an ECG lead as reference. Some datasets include data from healthy subjects: the dataset presented by Kaisti *et al.*[24] contains simultaneous 3D accelerometer and gyroscope recordings; the CEBS dataset[25–27] provides long-term SCG recordings; the multichannel seismocardiography dataset[28,29] contains simultaneous recordings from a matrix of accelerometers placed onto the thorax; the SensSmartTech dataset[30] provides simultaneous ECG, PCG, PPG, and accelerometer recordings. Other datasets include data from pathological subjects: the dataset presented by Yang and Tavassolian[31,32] and the SCG-RHC dataset[27,33,34] provide signals from patients with valvular heart disease and heart failure, respectively. Additionally, several heart sound datasets[27,35,36] provide simultaneous PCG and ECG recordings. Table 1 summarizes the main characteristics of these datasets of cardiomechanical signals, highlighting the number of subjects included, their health status, the type of signals recorded, and some limitations.

These datasets show inherent limitations. The vibrations and sounds generated by the heartbeat cover a rather wide frequency band ranging from the slow chest movements that can be felt by palpation at each heartbeat

[1]Department of Electrical Engineering and Information Technologies, University of Naples Federico II, Via Claudio, 21, 80125, Naples, Italy. [2]Department of Advanced Biomedical Sciences, University of Naples Federico II, Via Sergio Pansini, 5, 80131, Naples, Italy. [3]School of Engineering, Design and Built Environment, Western Sydney University, Penrith, NSW 2751, Australia. ✉e-mail: jessica.centracchio@unina.it

Dataset	Subjects	Male	Female	Signals	Limitations
CEBS[25]	Healthy	12	8	ECG, SCG, respiration	Unbalanced gender distribution Small sample size No heart sound data
Mechanocardiograms with ECG reference[24]	Healthy	29	0	ECG, SCG, GCG	Only male participants No heart sound and respiration
Multichannel Seismo-cardiography[28]	Healthy	13	0	ECG, SCG, respiration	Small sample size, only males No heart sound data Bulky instrumentation
SensSmartTech[30]	Healthy	14	18	ECG, SCG, PCG, PPG	Short duration of the recording No respiration data
Cardio-mechanical Signals from Patients with Valvular Heart Diseases[32]	Pathological	59	41	ECG, SCG, GCG	Unbalanced gender distribution No heart sound and respiration
SCG-RHC[33]	Pathological	49	24	ECG, SCG	Unbalanced gender distribution No heart sound and respiration
EPHNOGRAM[35]	Healthy	24	0	ECG, PCG	Small sample size, only males No heart sound and respiration
Radar-Recorded Heart Sounds[36]	Healthy	7	4	ECG, PCG	Unbalanced gender distribution Small sample size No heart sound and respiration

Table 1. Summary of various datasets used in cardiovascular research, highlighting participant demographics, signals included, and major limitations.

(from 0.5 Hz), up to the heart sounds (hundreds of Hz). The amplitude and morphology of vibrations and heart sounds are continuously modulated by respiration. Accelerometers can capture with good signal-to-noise ratio only inaudible vibrations in a frequency band ranging from 7 to 30 Hz. Lower frequencies are usually filtered out because they are associated with extremely low accelerations; higher frequencies (i.e., audio frequencies) generate much higher accelerations that are conventionally removed with built-in low-pass filters. Variations in the components of static gravitational acceleration can be used to monitor chest expansions due to respiration. Gyroscopes exhibit similar limitations, while stethoscope microphones capture only heart sounds (frequencies from 20–30 Hz to thousands of Hz).

The recent FCG technique[37–41] uses a single force sensor to acquire simultaneous measurements of chest oscillations, vibrations, and sounds, covering a wide frequency range from tenths to hundreds of Hz. Simple filtering operations can be used to decompose the raw FCG signal in several components related to the chest expansions and contractions due to respiration, the slow oscillations produced by heart walls displacements, the subsonic vibrations due to heart valves activity (very similar to SCG and GCG), and the heart sounds (as captured by stethoscopes). FCG allows prolonged and continuous monitoring of both cardiac and respiratory mechanical activity using a single lightweight sensor that can be embedded in clothes and apparels, thus enabling pervasive monitoring applications. To date, there is no public database of FCG signals.

FOSTER is the first ever dataset of FCG signals. It contains also SCG, PCG, ECG, and respiration signals, which were recorded simultaneously to FCG signals from each subject. The FOSTER dataset offers a unique and unprecedented resource for researchers, enabling in-depth exploration of cardiac mechanics, performance comparison of different cardiomechanical techniques for diagnostic purposes, assessment of cardiac and respiratory parameters against reference ECG and respiratory signals.

Methods

Participants. The dataset population consists of 40 healthy subjects (20 males and 20 females), aged 26.93 ± 7.09 years. The age distribution is depicted in Fig. 1. Data were collected at the Hypertension Centre of AOU Federico II (80131, Naples, Italy) between July 2024 and March 2025. The study was carried out in accordance with the Declaration of Helsinki and approved by the Ethical Committee "Università Federico II - AORN A. Cardarelli" (prot. nr. 0015104, date: 28 March 2023). Informed consent was obtained from all subjects involved in the study. Personal data have been anonymized to ensure the non-traceability of individuals involved. Age and gender data were maintained. The participants consented to the use of their anonymized data for clinical studies and for sharing and publication in scientific articles.

Signals recording. Each subject sat comfortably in a chair and was invited to place his or her back against the backrest and the forearms on the armrests and to remain relaxed. The placement of the sensors used to acquire the physiological signals is schematized in Fig. 2. The FCG signal was acquired by a pair of piezoelectric sensors placed on top of each other, specifically a lead-zirconate-titanate (PZT) sensor and a polyvinylidene fluoride (PVDF) sensor, as described in a previous study[41].

An ADXL335 accelerometer (Analog Devices, inc.) was stacked on top of the two piezoelectric sensors structure, in order to record the SCG signal from the same site on the chest: details of this arrangement can be found in a previous study[41]. Only the dorsoventral component of the acceleration was recorded since it is the most widely used for seismocardiography. The FCG-SCG sensors assembly was positioned on the fourth intercostal space between the sternal line and the mid-clavicular line, identifying the point of maximal signal amplitude for each subject (see Fig. 2). An Aethra Telestethphone electronic stethoscope, featuring Littmann chestpiece and tubing, was used to record heart sounds. The stethoscope chestpiece was placed as close as possible to the

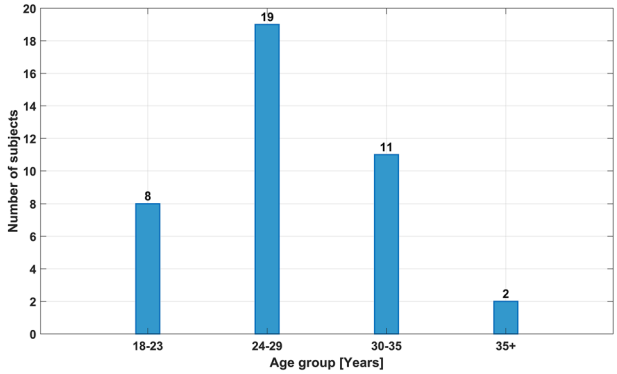

Fig. 1 Age distribution of the FOSTER dataset population.

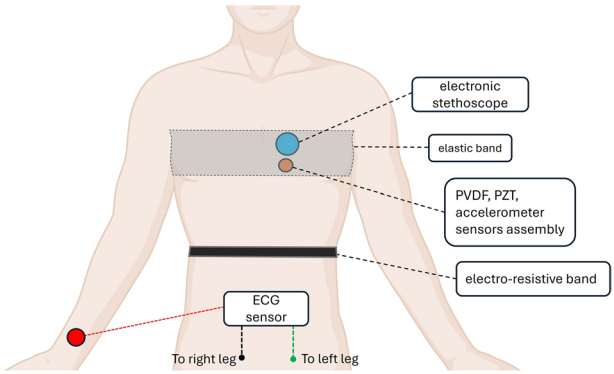

Fig. 2 Measurement setup used in data acquisition of the FOSTER dataset.

FCG sensor (see Fig. 2). These sensors were attached to the subject's chest via an elastic belt wrapped around the chest. The reference ECG lead II was acquired using a WelchAllyn Propaq® Encore monitor (Welch Allyn Inc., New York, NY, USA). The reference respiratory signal was captured via an electro-resistive band (ERB)[42] placed around the subject's abdomen as showed in Fig. 2.

All signals were synchronously recorded via a National Instrument NI-USB6212 DAQ board (National Instruments Corp., Austin, TX, USA) with a sampling frequency of 10 kHz and 16-bit precision for approximately 7 minutes. The frequency content of the acquired signals, which included the heart sounds, is less than 1 kHz. The 10 kHz sampling rate ensured a very fine time resolution in order to allow accurate cardiac time intervals measurements. Each subject was asked to alternate phases of quite breathing and apneas. The first 5 minutes of the recording involved calm, spontaneous breathing. Then, participants were asked to perform an inspiratory apnea, followed by a short breathing period, and finally an expiratory apnea. Figure 3a shows an excerpt of all signals recorded, where phases of quiet breathing and apnea are clearly visible. Figure 3b, on the other hand, shows an excerpt of each signal during quiet breathing on a different timescale, where individual heartbeat and respiration acts are clearly recognizable.

Data Records

The FOSTER dataset is available at an Open Science Framework repository[43] https://osf.io/3u6yb/. The dataset is structured to facilitate analysis and usability of the data. A single comma separated values (CSV) file is provided for each subject, named "sub0xx", where xx represents the numbering associated with each subject. Each CSV file consists of seven fields, described in Table 2. The demographic information, including age, sex, and to be smoker, is collected in a separate file. To support researchers in accessing and analyzing data, MATLAB® code is also provided.

Technical Validation

Technical validation of the dataset was performed by first assessing the quality of the data via the estimation of signal-to-noise ratio (SNR) and by evaluating the error associated with the estimation of key vital signs, such as the instantaneous heart rate and respiratory rate. This analysis provides evidence of signals quality and consistency with respect to the reference signals. MATLAB® R2023b (The MathWorks, Inc., 1 Apple Hill Drive, Natick, Massachusetts, 01760, United States) was used for all signal processing and analysis procedures.

SNR estimation. The Signal-to-Noise Ratio (SNR) was estimated in the frequency domain using power spectral density (PSD) analysis[44]. SNR was calculated by assuming that the noise floor of the signals is white noise, which is characterized by a constant PSD across frequencies. PSD of combined signal and noise (PSD_{SN})

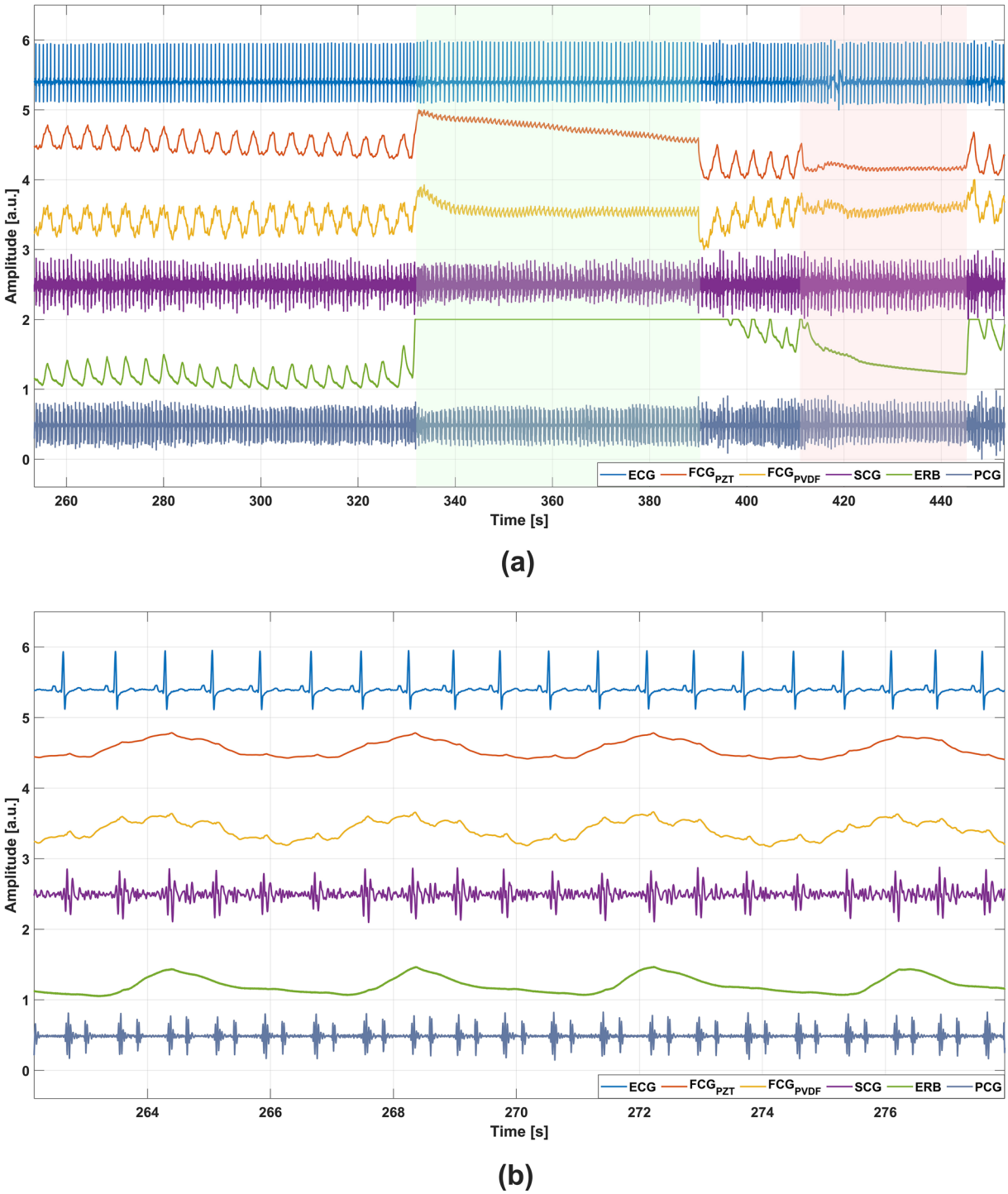

Fig. 3 An excerpt of signals acquired from subject #018. The six recorded signals represented from top to bottom are: ECG (blue); FCG_{PZT} (red); FCG_{PVDF} (orange); SCG (violet); Respiration (green); PCG (grey). (**a**) a 200-seconds segment including quiet breathing and apnea phases; the graph area with green background corresponds to the inspiratory apnea, while the graph area with red background corresponds to the expiratory apnea; (**b**) a 14-seconds segment including 20 heartbeats and 4 respiratory cycles during quiet breathing.

was computed by squaring the amplitude spectrum of the Fourier Transform. The total power of combined signal and noise (P_{SN}) was obtained by summing all PSD_{SN} values. The signals were sampled at 10 kHz. The frequency band between 1 kHz to 5 kHz, was assumed to contain only noise with no signal activity and was selected to quantify the withe noise intensity (see Fig. 4). The noise power in [1–5] kHz ($P_{N\ [1-5]\ kHz}$) was obtained by summing all PSD_N values in that frequency band. To estimate the PSD of the noise (PSD_{Nest}), $P_{N\ [1-5]\ kHz}$ was divided by the noise bandwidth. This gave an estimate of the noise's spectral density within the noise-only frequency range. Once

File name	Column	Content
sub0xx.csv	1	Time [s]
	2	ECG signal
	3	FCG raw signal from PVDF sensor
	4	FCG raw signal from PZT sensor
	5	SCG signal
	6	PCG signal
	7	Respiration signal from ERB

Table 2. Description of the data structure in the CSV files. Each file (sub0xx.csv) contains multiple columns, where each column corresponds to a specific recorded signal. The first column represents the sampling times reported in seconds, while the remaining columns store the physiological signals acquired from the different sensors, including ECG, PVDF, PZT, SCG, PCG, and ERB.

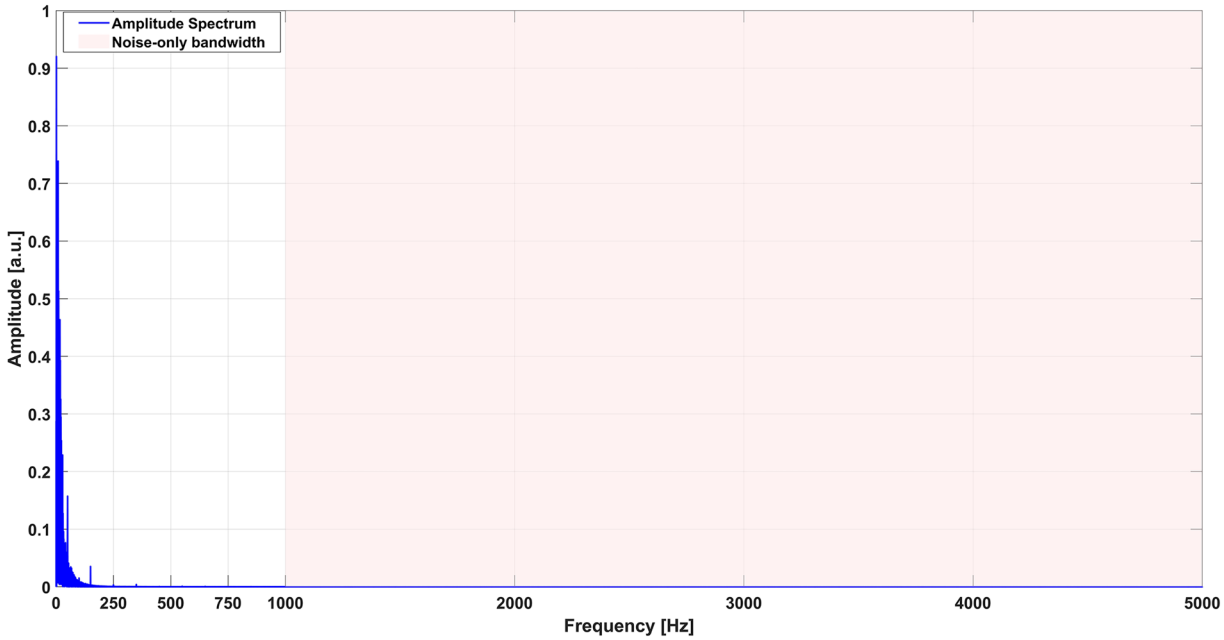

Fig. 4 Amplitude spectrum of ECG signal of subject #006. The shaded region (1–5 kHz) represents the frequency band used to estimate the power spectral density (PSD) of the noise. This range is assumed to contain only noise components, ensuring a reliable estimation of the noise floor.

the PSD_{Nest} was obtained, it was multiplied by the total frequency range (which is half of the sampling frequency, fs/2) to obtain the total noise power (P_{Ntot}). This extended the noise power estimate across the entire frequency spectrum. To compute the signal power, P_{Ntot} was subtracted from (P_{SN}), yielding the total signal power $P_{Stot.}$ Finally, the SNR expressed in dB was calculated by the following expression:

$$SNR = 10 \cdot \log_{10}\left(\frac{P_{Stot}}{P_{Ntot}}\right) \quad (1)$$

To ensure that the noise floor can be considered white noise, the slope of $PSD_{N\,[1-5]\,kHz}$ range was computed. Additionally, the standard deviation of the $PSD_{N\,[1-5]\,kHz}$ was calculated to assess the variability of the spectrum in the selected range. The SNR values and $PSD_{N\,[1-5]\,kHz}$ slopes were computed separately for each signal type in the database for each subject. Finally, the mean and standard deviation (SD) of all SNR values for each signal type were calculated for each subject. The same statistical analysis was performed for the $PSD_{N\,[1-5]\,kHz}$ slope values.

FCG components extraction. The raw FCG signal consists of a large, dominant respiratory component (also named Force-RespiroGram - FRG) and much smaller cardiac components superimposed. To extract the cardiac FCG components, it is first necessary to separate the large FRG component from the smaller cardiac component of the FCG signal. A 21st-order Savitzky-Golay filter[45] with a frame length between 8 and 18 seconds was used for the extraction of the FRG. Then, the FRG was subtracted from the raw FCG signal to isolate the

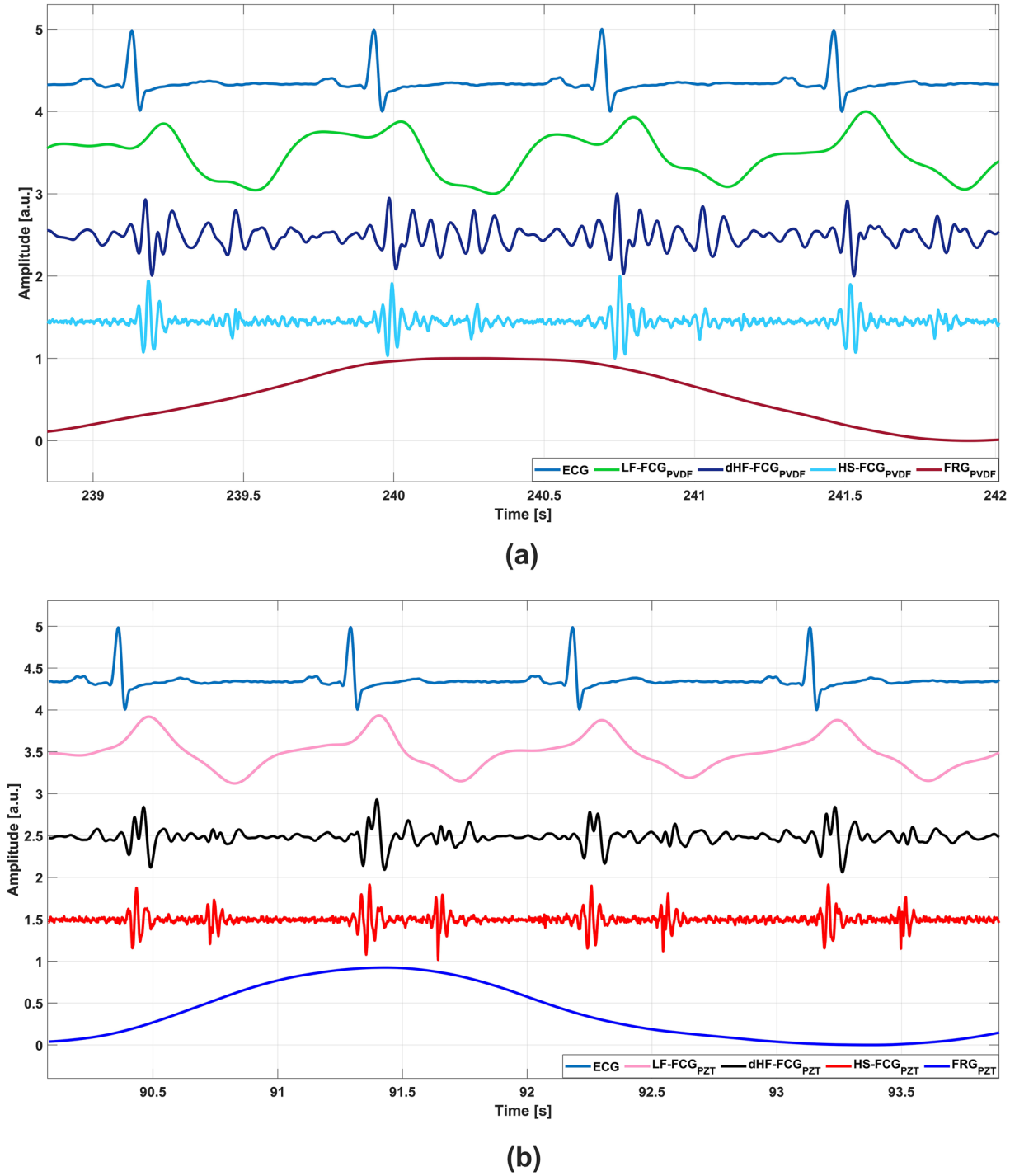

Fig. 5 Excerpt of cardiac components extracted from FCG raw signals, with FRG, and ECG signals from subject #018: (**a**) PVDF sensor signals; (**b**) PZT sensor signals.

cardiac components, which were further separated via band-pass filtering. In particular, the LF-FCG component was obtained by filtering in the 0.5–6 Hz band, the HF-FCG component by filtering in the 7–30 Hz band, and the HS-FCG component (i.e. the heart sounds) by filtering in the 30–300 Hz band. The first derivative of the HF-FCG (dHF-FCG) component was also computed, since it had previously been found to be highly similar to the SCG signal[39]. As an example, Fig. 5 illustrates the FCG signal components extracted from the raw FCG signals acquired by PZT and PVDF sensors, along with the ECG signals. While HF-FCG and HS-FCG are related to valves activities, the LF-FCG is related to the filling and emptying of the heart chambers during the cardiac cycle.

Physiological parameters estimation. Common applications include estimating heart rate and respiratory rate. FCG signals captured by PVDF and PZT sensors were analyzed and compared with the

N	Parameters		Signals					
			ECG	FCG_{PVDF}	FCG_{PZT}	SCG	PCG	ERB
40	SNR [dB]	mean	81.52	70.27	73.02	83.73	31.35	75.35
		SD	1.25	7.20	6.19	0.53	6.47	5.02
	$SLOPE_{PSD}$ [dB/Hz]	mean	−0.00002	−0.00011	−0.00054	−0.00002	−0.00037	0.00053
		SD	0.000068	0.000189	0.00056	0.000002	0.000270	0.001952

Table 3. Summary of the SNR and PSDN slope for each signal type in the dataset. PSD is evaluated in the noise-only frequency range.

Signal	Components	Reference heartbeats	TPs	FPs	FNs	Sensitivity (%)	PPV (%)
FCG	dHF-FCG_{PVDF}	17104	16018	459	1086	94.0	97.0
	dHF-FCG_{PZT}	17104	15847	451	1257	92.6	97.2
	HS-FCG_{PVDF}	17104	13214	2254	3890	77.3	85.4
	HS-FCG_{PZT}	17104	13090	1526	4014	76.5	89.6

Table 4. The overall results of statistical analysis in heartbeat detection for FCG signal components across all subjects.

Signal	Components	N_{IBIs}	R^2	Slope	CI_{slope}	Intercept (ms)	$CI_{intercept}$(ms)
FCG	dHF-FCG_{PVDF}	15245	>0.99	1.001	[1.001; 1.001]	−0.648	[−0.927; −0.369]
	dHF-FCG_{PZT}	14979	>0.99	1.002	[1.001; 1.002]	−1.219	[−1.527; −0.912]
	HS-FCG_{PVDF}	11083	>0.99	1.001	[1.001; 1.002]	−0.933	[−1.223; −0.643]
	HS-FCG_{PZT}	11021	>0.99	1.002	[1.001; 1.002]	−1.307	[−1.649; −0.965]

Table 5. The overall results of linear regression and correlation analyses on inter-beat intervals estimation obtained from ECG signal and FCG signal components across all subjects.

Signal	Components	N_{IBIs}	bias (ms)	CI_{bias}(ms)	LoA (ms)	$CI_{LoA\ min}$(ms)	$CI_{LoA\ max}$(ms)
FCG	dHF-FCG_{PVDF}	15245	0.00	[0.00; 0.100]	[−5.500; 5.100]	[−5.600; −5.300]	[5.000; 5.300]
	dHF-FCG_{PZT}	14979	0.00	[0.00; 0.100]	[−6.000; 5.803]	[−6.200; −5.700]	[5.600; 6.100]
	HS-FCG_{PVDF}	11083	0.00	[−0.100; 0.00]	[−4.500; 4.600]	[−4.700; −4.363]	[4.400; 4.800]
	HS-FCG_{PZT}	11021	0.10	[0.00; 0.100]	[−5.300; 4.800]	[−5.600; −5.100]	[4.530; 5.130]

Table 6. The overall results of Bland-Altman analysis on inter-beat intervals estimation obtained from ECG signal and FCG signal components across all subjects. Since the inter-beat intervals measurement differences were distributed with a non-normal distribution, the bias was estimated as the median of differences and the limits of agreement as the 2.5th and 97.5th percentiles, respectively.

reference ECG and respiratory signals. In particular, inter-beat and inter-breath intervals were estimated by FCG signals and then compared with those provided by reference ECG and ERB signals, to demonstrate data quality and the reliability of cardio-respiratory monitoring and analysis. The analyses involved the quiet breathing phases. Heartbeats were detected from ECG signals via the well-known Pan-Tompkins algorithm[46]. Heartbeats from dHF-FCG and HS-SCG signals were detected via a fully automatic template matching approach[40,47–51]. After heartbeats localization, correct heartbeat detections (true positives, TPs), false heartbeat detections (false positives, FPs) and missed heartbeats (false negatives, FNs) were annotated with the support of the reference ECG signals. Inter-beat intervals (IBIs) were then estimated as the time difference between consecutive heartbeats and compared with those provided by the reference ECG signal. Similarly, respiratory acts were identified in the FRG components (extracted from FCG raw signals) via the MATLAB® function *findpeaks*. TPs, FPs and FNs were annotated with the support of the reference ERB signals. The inter-breath intervals (IBrIs) were estimated as the time difference between consecutive respiratory acts and then compared with those obtained from the ERB signal. Regression correlation and Bland-Altman analysis[52,53], implemented in the MATLAB® function *bland–altman-and-correlation-plot*[54], were used to compare the IBIs and IBrIs estimated by FCG signals to those provided by reference ECG and ERB signals. Finally, the histograms of errors on IBIs and IBrIs estimates obtained from the reference signals and FCG signals were calculated. To ensure accuracy, inter-beat and inter-breath intervals corrupted by FPs and FNs were excluded from the analyses. Additionally, sensitivity and positive predictive value (PPV) were used as metrics to assess the performance of the algorithms used for heart-beat and respiratory acts detection.

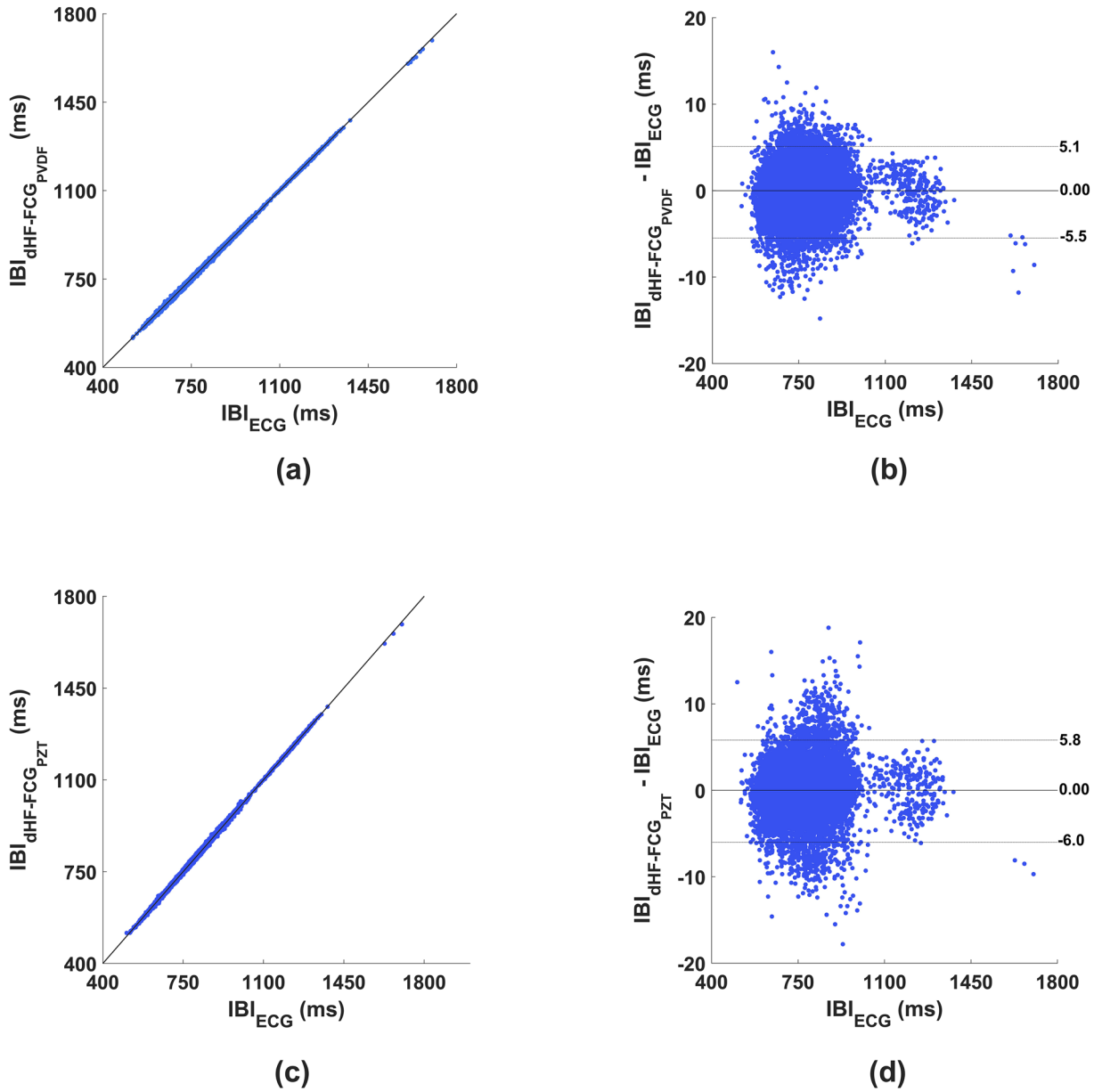

Fig. 6 Statistical analyses on the inter-beat intervals (IBIs) obtained from dHF-FCG signals (extracted from the PVDF and PZT sensor signal) and reference ECG signals: (**a**) results of regression and correlation analysis achieved from $dHF\text{-}FCG_{PVDF}$ signal; (**b**) results of Bland–Altman analysis achieved from $dHF\text{-}FCG_{PVDF}$ signal; (**c**) results of regression and correlation analysis achieved from $dHF\text{-}FCG_{PZT}$ signal; (**d**) results of Bland–Altman analysis achieved from $dHF\text{-}FCG_{PZT}$ signal.

Performance assessment. *SNR results.* The mean SNR of the ECG signal across all subjects is 81.52 ± 1.25 dB, while the mean and standard deviation of the PSD_N slope in the noise-only frequency range are close to zero. FCG signals present an average SNR of more than 70 dB, with a standard deviation of less than 8 dB, and their PSD_N slope also presents a mean and standard deviation close to zero. SCG signals present an average SNR of 83.73 ± 0.53 dB, with the PSD_N slope maintaining values close to zero. For the respiratory signal (ERB), the mean SNR is 75.35 ± 5.02 dB, while both the mean and standard deviation of the PSD_N slope remain close to zero. A slightly lower, but still remarkable SNR is observed for PCG signals, which have an average SNR of 31.35 ± 6.4 dB, while the mean and standard deviation of the PSD_N slope remain close to zero. Table 3 summarizes the mean and standard deviation of the SNR and PSD_N slope values for each signal across all subjects in the dataset. The results achieved indicate that the PSD_N remains flat in the noise-only frequency band for all signals, suggesting that the noise is indeed white. This confirms that the SNR estimate is reliable.

Results of physiological parameters estimation: heart monitoring. Table 4 shows the number of heartbeats accurately identified (TP) on all subjects from FCG cardiac components, as well as the number of FPs, FNs. Table 4 also reports sensitivity and PPV values. Specifically, 16018 and 15847 heartbeats were correctly identified,

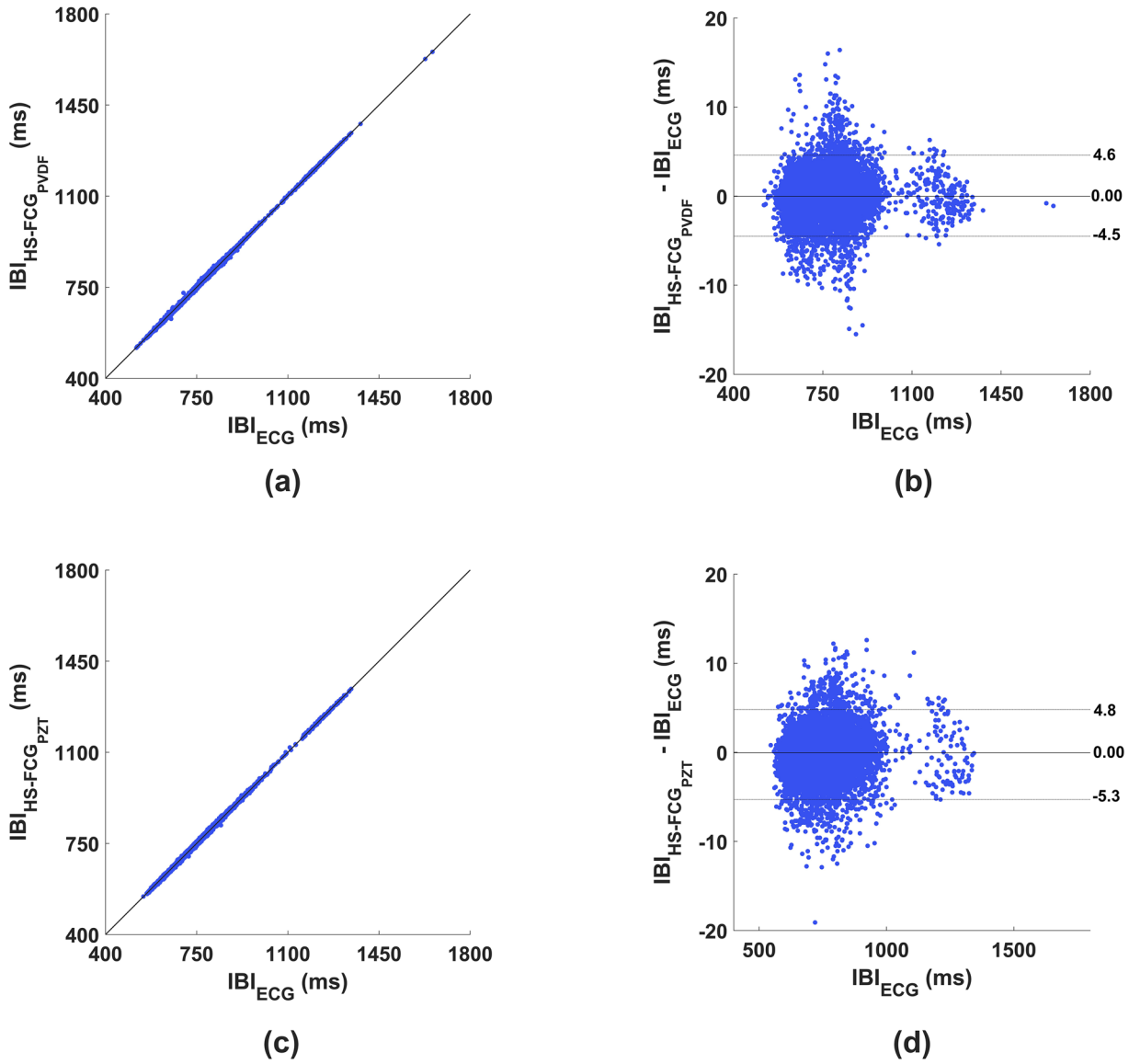

Fig. 7 Statistical analyses on the inter-beat intervals (IBIs) obtained from HS-FCG signals (extracted from the PVDF and PZT sensor signal) and reference ECG signals: (**a**) results of regression and correlation analysis achieved from HS-FCG$_{PVDF}$ signal; (**b**) results of Bland–Altman analysis achieved from HS-FCG$_{PVDF}$ signal; (**c**) results of regression and correlation analysis achieved from HS-FCG$_{PZT}$ signal; (**d**) results of Bland–Altman analysis achieved from HS-FCG$_{PZT}$ signal.

respectively, in dHF-FCG$_{PVDF}$ and dHF-FCG$_{PZT}$ signals, out of a total of 17104 reference heartbeats. A sensitivity and PPV of 94% and 97%, and of 93% and 97% were achieved, respectively, for dHF-FCG$_{PVDF}$ and dHF-FCG$_{PZT}$ signals. HS-FCG$_{PVDF}$ and HS-FCG$_{PZT}$ signals achieved a sensitivity and PPV of 77% and 85%, and of 77% and 90%, respectively. In fact, 13214 and 13090 heartbeats were correctly identified, respectively, in HS-FCG$_{PVDF}$ and HS-FCG$_{PZT}$ signals, out of a total of 17104 reference heartbeats. The overall results of the linear regression, correlation and Bland-Altman analysis are summarized in Tables 5, 6, as well as the confidence intervals (CIs) of the statistical parameters. Statistical analyses, performed on 15245 and 14979 IBIs estimated from both dHF-FCG$_{PVDF}$ and dHF-FCG$_{PZT}$ signals and ECG, showed a coefficient of determination (R^2) greater than 0.99, with unit slopes for both signals. The intercepts were −0.6 ms for dHF-FCG$_{PVDF}$ and −1.2 ms for dHF-FCG$_{PZT}$ (see Fig. 6a,c). Bland-Altman analysis showed a nonsignificant bias with a confidence interval (CI$_{bias}$) of [0.00; 0.100] ms for both dHF-FCG signals. Limits of agreement (LoA) ranged from −5.5 to 5.1 ms for dHF-FCG$_{PVDF}$ and from −6.0 to 5.8 ms for dHF-FCG$_{PZT}$, suggesting slightly higher variability for the second one (see Fig. 6b,d). Similarly, 11083 IBIs obtained from HS-FCG$_{PVDF}$ and 11021 from HS-FCG$_{PZT}$ signals were compared with those provided by the reference ECG. The linear regression results indicated an R^2 greater than 0.99 for both audible components, with slopes of 1.0 for HS-FCG$_{PVDF}$ and 1.0 for HS-FCG$_{PZT}$. The intercepts were slightly larger compared to dHF-FCG signals, with values of −0.9 ms for HS-FCG$_{PVDF}$ and −1.3 ms for HS-FCG$_{PZT}$, as shown in Fig. 7a,c. The Bland-Altman analysis showed a nonsignificant bias for both HS-FCG signal with CI$_{bias}$ of [−0.1;

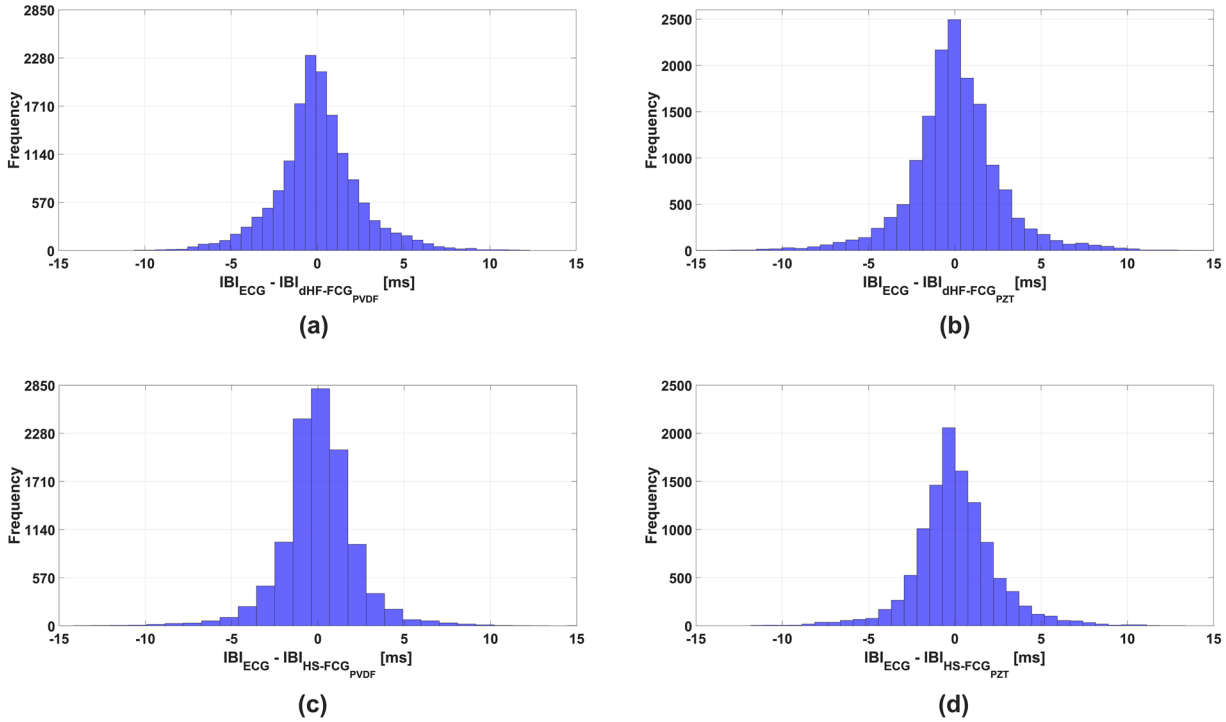

Fig. 8 Histograms of the errors on the IBI estimates between the reference ECG signal and the FCG signal components: (**a**) histogram of errors on IBIs between ECG and dHF-FCG$_{PVDF}$; (**b**) histogram of errors on IBIs between ECG and dHF-FCG$_{PZT}$; (**c**) histogram of errors on IBIs between ECG and HS-FCG$_{PVDF}$; (**d**) histogram of errors on IBIs between ECG and HS-FCG$_{PZT}$.

0.1] ms for HS-FCG$_{PVDF}$ and [0.0; 0.1] ms for HS-FCG$_{PZT}$. The limits of agreement ranged from −4.5 to 4.6 ms for HS-FCG$_{PVDF}$ and from −5.3 to 4.8 ms for HS-FCG$_{PZT}$ (see Fig. 7b,d), suggesting that the HS-FCG signals exhibited slightly lower variability than dHF-FCG signals.

Figure 8 shows the histograms of the errors on the IBIs estimates between the reference ECG signal and the FCG signal components. The histograms of errors exhibit a gaussian distribution centered around zero, indicating that the measurement errors are symmetrically distributed with no significant bias. This suggests that the estimated values are, on average, very close to the reference values, with errors randomly distributed around zero. These results demonstrate the reliability of the recorded FCG data for heartrate monitoring applications.

Results of physiological parameters estimation: respiration monitoring. Table 7 shows the number of respiratory acts accurately identified (TPs) on all subjects by FCG respiratory components (FRG) provided by PVDF and PZT sensors, as well as the number of FPs and FNs. Sensitivity and PPV values are also reported in Table 7. Overall, out of a total of 3472 reference respiratory acts provided by the ERB signal, 3299 were accurately detected from the FRG$_{PVDF}$ signals and 3244 from the FRG$_{PZT}$ signals. Sensitivity and PPV were 95% and 92.4% for FRG$_{PVDF}$ signals, and 93.4% and 92.6% for FRG$_{PZT}$ signals. The overall results of the linear regression, correlation, and Bland-Altman analysis were outlined in Tables 8, 9. For the FRG$_{PVDF}$ component, the results of the linear regression and correlation analysis performed on 3128 IBrIs show strong agreement with the reference ERB signal. The coefficient of determination (R^2) was 0.964 and the slope was close to unity (0.994), indicating an almost perfect proportional relationship. The intercept was minimal (0.017 s), with a confidence interval ranging from −0.008 to 0.042 s (see Fig. 9a). Bland-Altman analysis further supports these results, with a non-significant bias with CI$_{bias}$ of [−0.0082; 0.0017] s. The limits of agreement (LoA) ranged from −0.505 to 0.504 s (see Fig. 9b).

For the FRG$_{PZT}$ component, the agreement with the reference ERB signal remained strong, although slightly lower than FRG$_{PVDF}$. As shown in the Fig. 10a the R^2 value was 0.958, with a slope of 0.988, still close to unity and an intercept of 0.041 s. Bland-Altman analysis revealed a nonsignificant bias, with CI$_{bias}$ of [−0.0079; 0.0022] s. The limits of agreement (LoA) ranged from −0.550 to 0.557 s (see Fig. 10b). Furthermore, the analysis of the error distributions across the histograms revealed that the errors followed a gaussian distribution centered around zero for both respiratory components, FRG$_{PVDF}$ and FRG$_{PZT}$ (see Fig. 11). This further supports the reliability of the measurements, as it suggests that the estimation errors are unbiased and not due to systematic deviations. These results also demonstrate the reliability of the recorded FCG data for respiratory monitoring applications.

Signal	Components	Reference acts	TPs	FPs	FNs	Sensitivity (%)	PPV (%)
FCG	FRG_{PVDF}	3472	3299	273	173	95.0	92.4
	FRG_{PZT}	3472	3244	259	228	93.4	92.6

Table 7. The overall results of statistical analysis in respiratory acts detection for respiratory components of FCG signals across all subjects.

Signal	Components	N_{IBrIs}	R^2	Slope	CI_{slope}	Intercept (s)	$CI_{intercept}$(s)
FCG	FRG_{PVDF}	3128	0.964	0.994	[0.988; 1.001]	0.017	[−0.008; 0.042]
	FRG_{PZT}	3075	0.958	0.988	[0.981; 0.995]	0.041	[0.013; 0.069]

Table 8. The overall results of linear regression and correlation analyses on inter-breath intervals estimations obtained from ERB signal and FCG respiratory components across all subjects.

Signal	Components	N_{IBrIs}	bias (s)	CI_{bias}(s)	LoA (s)	$CI_{LoA\ min}$(s)	$CI_{LoA\ max}$(s)
FCG	FRG_{PVDF}	3128	−0.003	[−0.0082; 0.0017]	[−0.505; 0.504]	[−0.564; −0.456]	[0.467; 0.590]
	FRG_{PZT}	3075	−0.003	[−0.0079; 0.0022]	[−0.550; 0.557]	[−0.608; −0.496]	[0.490; 0.633]

Table 9. The overall results of Bland-Altman analysis on inter-breath intervals estimation obtained from ERB signal and FCG respiratory components across all subjects. Since the inter-breath intervals measurement differences were distributed with a non-normal distribution, the bias was estimated as the median of differences and the limits of agreement as the 2.5th and 97.5th percentiles, respectively.

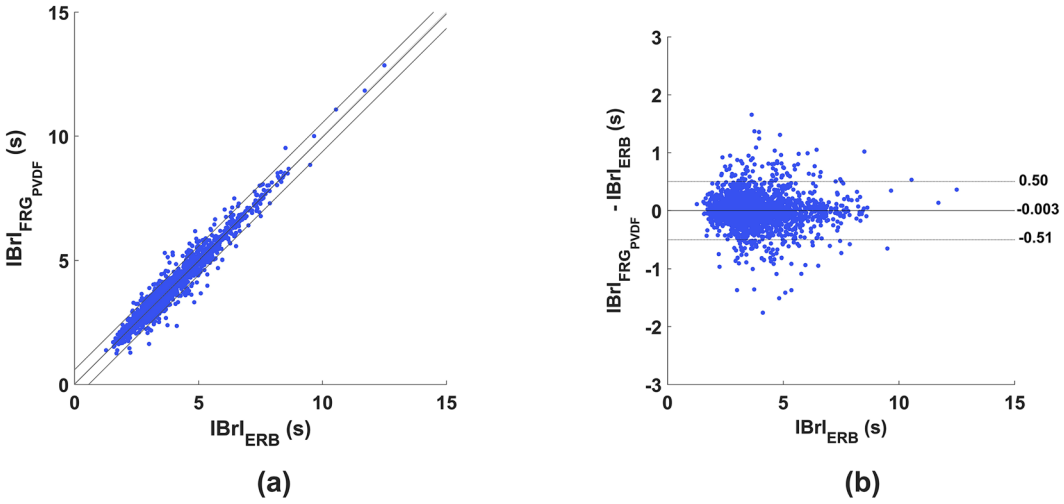

Fig. 9 Statistical analyses on the inter-breath intervals (IBrIs) obtained from ERB and FRG_{PVDF} signals: (**a**) results of regression and correlation analyses; (**b**) results of Bland–Altman analysis.

Usage Notes

This dataset, which comprises various physiological signals including electrocardiograms (ECG), Forcecardiograms (FCG), Seismocardiograms (SCG), Phonocardiograms (PCG), and respiratory signals, offers vast potential in a wide range of clinical and research applications. The inclusion of the FCG signal is particularly noteworthy, as it inherently incorporates information provided by all other mechanical signals in the dataset. This makes FCG exceptionally helpful for comprehensive cardio-respiratory analysis. By leveraging FCG signals, it is possible to assess key cardiac parameters with high accuracy. For example, using automated algorithms, cardiac time intervals, such as pre-ejection period (PEP), can be estimated with remarkable accuracy[39]. Additionally, FCG-based algorithms can precisely localize heart sounds, which are essential for accurate diagnosis and monitoring of heart conditions[40]. The dataset also enables the extraction of short-term indices of heart rate variability (HRV), a key metric in cardiovascular health assessment[50,55]. Moreover, the combination of respiratory and cardiac signals can be very useful for monitoring and diagnosing various cardiorespiratory conditions, such as sleep apnea, heart failure, and arrhythmias. Respiratory signals can be integrated with other cardiovascular data to provide a more holistic view of an individual's health status, improving both diagnostics and treatment protocols. Beyond clinical monitoring, this dataset also holds significant potential for the development and testing of artificial intelligence models that can automate cardio-respiratory analyses. Its versatility

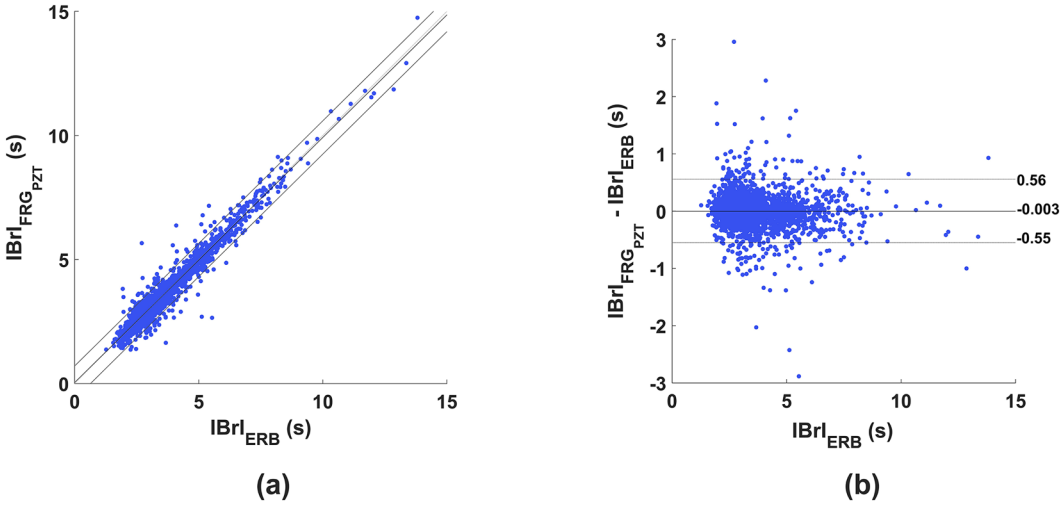

Fig. 10 Statistical analyses on the inter-breath intervals (IBrIs) obtained from ERB and FRG_{PZT} signals: (**a**) results of regression and correlation analyses; (**b**) results of Bland–Altman analysis.

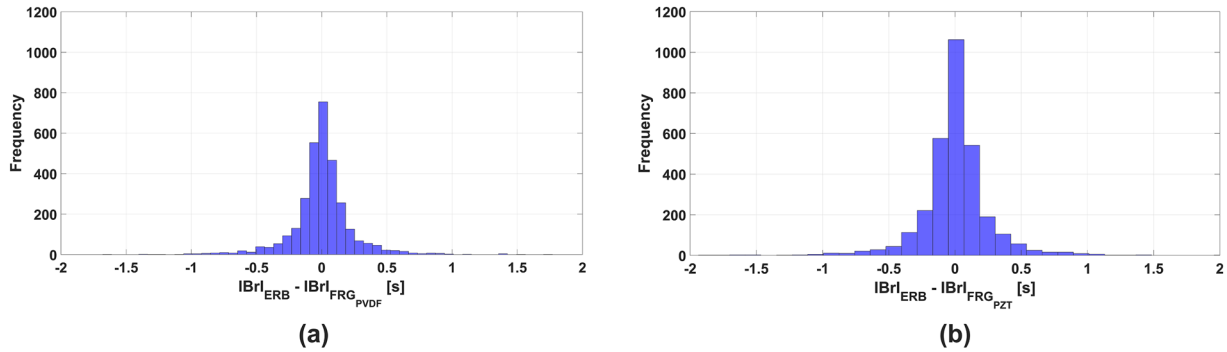

Fig. 11 Histograms of the errors on the IBrI estimates between the reference ERB signal and the FRG signal component: (**a**) histogram of errors on IBrIs between ERB and FRG_{PVDF}; (**b**) histogram of errors on IBrIs between ECG and FRG_{PZT}.

spans from cardiorespiratory monitoring to the development and testing of advanced artificial intelligence algorithms aimed at improving diagnostic accuracy and clinical decision-making. In conclusion, the FOSTER dataset offers a wealth of opportunities across various fields, including personalized medicine, clinical diagnostics, medical device development, and AI-driven health solutions. Its comprehensive nature makes it an invaluable resource for advancing both fundamental research and applied technologies in the realm of cardio-respiratory health monitoring.

This dataset can be easily imported into both MATLAB® and Python, making it accessible for data analysis and signal processing. To support preprocessing of the data, a MATLAB® code is also provided to extract and analyze all signals contained in the FOSTER dataset.

Code availability

The custom code used to access and analyze this dataset is available at an Open Science Framework repository https://osf.io/bd2gy/.

Received: 29 April 2025; Accepted: 24 July 2025;
Published online: 06 August 2025

References

1. Salerno, D. M. Seismocardiography: A New Technique for Recording Cardiac Vibrations. Concept, Method, and Initial Observations. *Journal of Cardiovascular Technology* **9**, 111–118 (1990).
2. Zanetti, J. M. & Tavakolian, K. Seismocardiography: past, present and future. *Annu Int Conf IEEE Eng Med Biol Soc* **2013**, 7004–7007 (2013).
3. Inan, O. T. *et al.* Ballistocardiography and Seismocardiography: A Review of Recent Advances. *IEEE Journal of Biomedical and Health Informatics* **19**, 1414–1427 (2015).
4. Taebi, A., Solar, B. E., Bomar, A. J., Sandler, R. H. & Mansy, H. A. Recent Advances in Seismocardiography. *Vibration* **2**, 64–86 (2019).

5. Jafari Tadi, M. *et al*. Gyrocardiography: A New Non-invasive Monitoring Method for the Assessment of Cardiac Mechanics and the Estimation of Hemodynamic Variables. *Sci Rep* **7**, 6823 (2017).
6. Sieciński, S., Kostka, P. S. & Tkacz, E. J. Gyrocardiography: A Review of the Definition, History, Waveform Description, and Applications. *Sensors* **20**, 6675 (2020).
7. Wells, B. Phonocardiography. *Br Med J* **2**, 9–10 (1954).
8. Rappaport, M. B. & Sprague, H. B. The graphic registration of the normal heart sounds. *American Heart Journal* **23**, 591–623 (1942).
9. Ismail, S., Siddiqi, I. & Akram, U. Localization and classification of heart beats in phonocardiography signals —a comprehensive review. *EURASIP J. Adv. Signal Process.* **2018**, 26 (2018).
10. Gordon, J. W. Certain Molar Movements of the Human Body produced by the Circulation of the Blood. *J Anat Physiol* **11**, 533–536 (1877).
11. Burger, H. C. & Noordergraaf, A. Physical basis of ballistocardiography. III. *Am Heart J* **51**, 179–185 (1956).
12. Deuchar, D. C. Ballistocardiography. *Br Heart J* **29**, 285–288 (1967).
13. Starr, I. The relation of the ballistocardiogram to cardiac function. *The American Journal of Cardiology* **2**, 737–747 (1958).
14. Knoop, A. A. Experimental investigations on ultra-low frequency displacement ballistocardiography. Nasa TT F-269. *NASA Contract Rep NASA CR* 1–107 (1965).
15. Sadek, I., Biswas, J. & Abdulrazak, B. Ballistocardiogram signal processing: a review. *Health Inf Sci Syst* **7**, 10 (2019).
16. Vogt, E., MacQuarrie, D. & Neary, J. P. Using ballistocardiography to measure cardiac performance: a brief review of its history and future significance. *Clinical Physiology and Functional Imaging* **32**, 415–420 (2012).
17. Etemadi, M. & Inan, O. T. Wearable ballistocardiogram and seismocardiogram systems for health and performance. *Journal of Applied Physiology* **124**, 452–461 (2018).
18. Castiglioni, P., Faini, A., Parati, G. & Di Rienzo, M. Wearable Seismocardiography. in *2007 29th Annual International Conference of the IEEE Engineering in Medicine and Biology Society* 3954–3957, https://doi.org/10.1109/IEMBS.2007.4353199 (2007).
19. Yang, C. & Tavassolian, N. Combined Seismo- and Gyro-Cardiography: A More Comprehensive Evaluation of Heart-Induced Chest Vibrations. *IEEE Journal of Biomedical and Health Informatics* **22**, 1466–1475 (2018).
20. Shandhi, M. M. H. *et al*. Performance Analysis of Gyroscope and Accelerometer Sensors for Seismocardiography-Based Wearable Pre-Ejection Period Estimation. *IEEE Journal of Biomedical and Health Informatics* **23**, 2365–2374 (2019).
21. Yang, C., Tang, S. & Tavassolian, N. Utilizing Gyroscopes Towards the Automatic Annotation of Seismocardiograms. *IEEE Sensors Journal* **17**, 2129–2136 (2017).
22. D'Mello, Y. *et al*. Real-Time Cardiac Beat Detection and Heart Rate Monitoring from Combined Seismocardiography and Gyrocardiography. *Sensors* **19**, 3472 (2019).
23. Jafari Tadi, M., Koivisto, T., Pänkäälä, M. & Paasio, A. Accelerometer-Based Method for Extracting Respiratory and Cardiac Gating Information for Dual Gating during Nuclear Medicine Imaging. *International Journal of Biomedical Imaging* **2014**, 690124 (2014).
24. Kaisti, M. *et al*. Mechanocardiograms with ECG reference. *IEEE Dataport* https://doi.org/10.21227/vfcs-k196 (2018).
25. García-González, M. A., Argelagós-Palau, A., Fernández-Chimeno, M. & Ramos-Castro, J. Combined measurement of ECG, Breathing and Seismocardiograms (CEBS database). physionet.org https://doi.org/10.13026/C2KW23 (2013).
26. García-González, M. A., Argelagós-Palau, A., Fernández-Chimeno, M. & Ramos-Castro, J. A comparison of heartbeat detectors for the seismocardiogram. in *Computing in Cardiology 2013* 461–464 (2013).
27. Goldberger, A. L. *et al*. PhysioBank, PhysioToolkit, and PhysioNet: components of a new research resource for complex physiologic signals. *Circulation* **101**, E215–220 (2000).
28. Munck, K., Sørensen, K., Struijk, J. J. & Schmidt, S. E. Multichannel seismocardiography: an imaging modality for investigating heart vibrations. *Physiol. Meas.* **41**, 115001 (2020).
29. Munck, K., Sørensen, K., J. Struijk, J. & Schmidt, E. S. Multichannel Seismocardiography: An Imaging Modality for Investigating Heart Vibrations. *Mendeley Data* https://doi.org/10.17632/scn464x7xd.2 (2020).
30. Lazović, A. *et al*. SensSmartTech database of cardiovascular signals synchronously recorded by an electrocardiograph, phonocardiograph, photoplethysmograph and accelerometer. *PhysioNet* https://doi.org/10.13026/FY9P-N277 (2025).
31. Yang, C. *et al*. An Open-Access Database for the Evaluation of Cardio-Mechanical Signals From Patients With Valvular Heart Diseases. *Front. Physiol.* **12**, (2021).
32. Yang, C. *et al*. An Open-access Database for the Evaluation of Cardio-mechanical Signals from Patients with Valvular Heart Diseases. *Zenodo* https://doi.org/10.5281/zenodo.5279448 (2021).
33. Chan, M., Klein, L., Fan, J. & Inan, O. SCG-RHC: Wearable Seismocardiogram Signal and Right Heart Catheter Database. *PhysioNet* https://doi.org/10.13026/133D-PK11 (2025).
34. Shandhi, M. M. H. *et al*. Estimation of Changes in Intracardiac Hemodynamics Using Wearable Seismocardiography and Machine Learning in Patients With Heart Failure: A Feasibility Study. *IEEE Trans. Biomed. Eng.* **69**, 2443–2455 (2022).
35. Kazemnejad, A., Gordany, P. & Sameni, R. EPHNOGRAM: A Simultaneous Electrocardiogram and Phonocardiogram Database. *PhysioNet* https://doi.org/10.13026/TJTQ-5911 (2025).
36. Shi, K. *et al*. A dataset of radar-recorded heart sounds and vital signs including synchronised reference sensor signals. *Sci Data* **7**, 50 (2020).
37. Andreozzi, E. *et al*. Forcecardiography: A Novel Technique to Measure Heart Mechanical Vibrations onto the Chest Wall. *Sensors (Basel)* **20**, 3885 (2020).
38. Andreozzi, E., Gargiulo, G. D., Esposito, D. & Bifulco, P. A Novel Broadband Forcecardiography Sensor for Simultaneous Monitoring of Respiration, Infrasonic Cardiac Vibrations and Heart Sounds. *Front. Physiol.* **12**, (2021).
39. Centracchio, J., Andreozzi, E., Esposito, D., Gargiulo, G. D. & Bifulco, P. Detection of Aortic Valve Opening and Estimation of Pre-Ejection Period in Forcecardiography Recordings. *Bioengineering* **9**, 89 (2022).
40. Centracchio, J., Parlato, S., Esposito, D. & Andreozzi, E. Accurate Localization of First and Second Heart Sounds via Template Matching in Forcecardiography Signals. *Sensors* **24**, 1525 (2024).
41. Parlato, S. *et al*. A Flexible PVDF Sensor for Forcecardiography. *Sensors* **25**, 1608 (2025).
42. Jayarathna, T., Gargiulo, G. D. & Breen, P. P. Continuous Vital Monitoring During Sleep and Light Activity Using Carbon-Black Elastomer Sensors. *Sensors (Basel)* **20**, 1583 (2020).
43. Parlato, S., Centracchio, J., Cinotti, E. & Andreozzi, E. FOSTER dataset. *OSF* https://doi.org/10.17605/OSF.IO/3U6YB (2025).
44. Kay, S. M. *Modern Spectral Estimation: Theory And Application*. (Prentice Hall, 1988).
45. Savitzky, A. & Golay, M. J. E. Smoothing and Differentiation of Data by Simplified Least Squares Procedures. *Anal. Chem.* **36**, 1627–1639 (1964).
46. Pan, J. & Tompkins, W. J. A Real-Time QRS Detection Algorithm. *IEEE Transactions on Biomedical Engineering* **BME-32**, 230–236 (1985).
47. Parlato, S., Centracchio, J., Esposito, D., Bifulco, P. & Andreozzi, E. Fully automated template matching method for ECG-free heartbeat detection in cardiomechanical signals of healthy and pathological subjects. *Phys Eng Sci Med* https://doi.org/10.1007/s13246-025-01531-3 (2025).
48. Centracchio, J., Parlato, S., Esposito, D., Bifulco, P. & Andreozzi, E. ECG-Free Heartbeat Detection in Seismocardiography Signals via Template Matching. *Sensors* **23**, 4684 (2023).
49. Parlato, S., Centracchio, J., Esposito, D., Bifulco, P. & Andreozzi, E. Heartbeat Detection in Gyrocardiography Signals without Concurrent ECG Tracings. *Sensors* **23**, 6200 (2023).

50. Parlato, S., Centracchio, J., Esposito, D., Bifulco, P. & Andreozzi, E. ECG-Free Heartbeat Detection in Seismocardiography and Gyrocardiography Signals Provides Acceptable Heart Rate Variability Indices in Healthy and Pathological Subjects. *Sensors (Basel)* **23**, 8114 (2023).
51. Parlato, S., Muto, V. & Bifulco, P. Accurate ECG-Free Heartbeats Localization in Long-Lasting SCG Recordings. in *Advances in Digital Health and Medical Bioengineering* (eds. Costin, H.-N., Magjarević, R. & Petroiu, G. G.) 196–204, https://doi.org/10.1007/978-3-031-62520-6_23. (Springer Nature Switzerland, Cham, 2024).
52. Altman, D. G. & Bland, J. M. Measurement in Medicine: The Analysis of Method Comparison Studies. *Journal of the Royal Statistical Society Series D: The Statistician* **32**, 307–317 (1983).
53. Giavarina, D. Understanding Bland Altman analysis. *Biochem Med* **25**, 141–151 (2015).
54. Bland-Altman and Correlation Plot - File Exchange - MATLAB Central. https://it.mathworks.com/matlabcentral/fileexchange/45049-bland-altman-and-correlation-plot (2025).
55. Centracchio, J. & Muto, V. Heart Rate Variability Analysis on Forcecardiography Signals: A Preliminary Study. in *Advances in Digital Health and Medical Bioengineering* (eds. Costin, H.-N., Magjarević, R. & Petroiu, G. G.) 179–187, https://doi.org/10.1007/978-3-031-62520-6_21 (Springer Nature Switzerland, Cham, 2024).

Acknowledgements

The authors would like to acknowledge Medical Monitoring Solutions PTY LTD for supporting this research. This research was supported by the project "New multimodal CArdioREspiratory MOnitoring device to improve chronic patient management (CAREMODE) – Cod. Prog. PNRR-POC-2022-12376833 – CUP C63C22001310007", funded by European Union – Next Generation EU – PNRR M6C2 I2.1 – "Valorizzazione e potenziamento della ricerca biomedica del SSN".

Funded by the European Union
NextGenerationEU

Author contributions

Conceptualization, E.A., P.B.; methodology, S.P., J.C., E.C., E.A.; software, S.P., J.C., E.A.; investigation, S.P., J.C., E.C., M.V.M., G.C., M.P., M.L., B.M.B., G.D.G., P.B., G.E., R.I., E.A.; data curation, S.P., J.C., E.C., E.A.; writing—original draft preparation, S.P., P.B., E.A.; writing—review and editing, S.P., J.C., E.C., M.V.M., G.C., M.P., M.L., B.M.B., G.D.G., P.B., G.E., R.I., E.A.; visualization, S.P.; supervision, E.A.; project administration, R.I., E.A.; funding acquisition, M.L., P.B., R.I., E.A.

Competing interests

The forcecardiography sensors used to acquire the FCG signals described in this manuscript are protected by the patent WO/2021/072493. The electro-resistive bands used to acquire the respiratory signals described in this manuscript are protected by the patent WO/2015/077839. E.A., G.D.G., and P.B. are listed as inventors and are minority shareholders of Medical Monitoring Solutions PTY LTD, which owns the mentioned IPs. All the other authors declare no conflicts of interest.

Additional information

Correspondence and requests for materials should be addressed to J.C.

Reprints and permissions information is available at www.nature.com/reprints.

Publisher's note Springer Nature remains neutral with regard to jurisdictional claims in published maps and institutional affiliations.

Open Access This article is licensed under a Creative Commons Attribution-NonCommercial-NoDerivatives 4.0 International License, which permits any non-commercial use, sharing, distribution and reproduction in any medium or format, as long as you give appropriate credit to the original author(s) and the source, provide a link to the Creative Commons licence, and indicate if you modified the licensed material. You do not have permission under this licence to share adapted material derived from this article or parts of it. The images or other third party material in this article are included in the article's Creative Commons licence, unless indicated otherwise in a credit line to the material. If material is not included in the article's Creative Commons licence and your intended use is not permitted by statutory regulation or exceeds the permitted use, you will need to obtain permission directly from the copyright holder. To view a copy of this licence, visit http://creativecommons.org/licenses/by-nc-nd/4.0/.

© The Author(s) 2025